our Rule 1 we note here again that our rules are not applicable near the equator, where according to eqn (4.1) Ekman layer transport grows beyond all bounds. In practical applications eqn (4.1) is valid to within about 2° of the equator, where quite large Ekman transports do occur in response to quite modest wind stresses.

Ekman pumping

Wind-induced currents are among the strongest currents in the oceanic surface layer. More importantly, the depth-integrated Ekman transports rank among the most important causes of flow in the deeper layers as well, throughout the upper one or two kilometers of the ocean. This comes about because the Ekman transports converge in some regions and diverge in others, and vertical flow develops at the bottom of the surface boundary layer to replace or remove the converging water masses. This process of generation of flow below the surface layer through vertical movement into and out of it is known as Ekman pumping. Because of its importance for the distribution of hydrographic properties below the surface layer it is worth looking at this process in some detail.

We see from eqn (4.1) that variations of Ekman layer transport can result from two factors, the change of the Coriolis parameter with latitude and the structure of the wind stress field. In most situations the variation of f is small and Ekman pumping is dominated by spatial variations of wind stress. Figure 4.1 shows some examples. Between the Trades and the Westerlies (boxes *A* and *B*) the wind generates a mean flow into the box, resulting in Ekman pumping or downwelling. Poleward of the maximum Westerlies (box *C*) the net flow is directed outward, giving negative Ekman pumping ("Ekman suction") or upwelling. In all situations (except near the equator) the vertical velocity w at the base of the Ekman layer (positive for downwelling, negative for upwelling) is given by the divergence of the Ekman transport: $- \rho_o w = \partial M_e^x / \partial x + \partial M_e^y / \partial y$ where M_e^x and M_e^y are the components of M_e towards east and north respectively. From Rule 3 these components can be expressed, away from the equator, in terms of wind stress:

$$- \rho_o w = \text{curl} \, (\tau / f) = \partial \, (\tau_y / f) / \partial x - \partial \, (\tau_x / f) / \partial y \quad (4.2)$$

where τ_x and τ_y are the x- and y-components of τ. (The curl of a field of vectors is a vector which measures the tendency of the vectors to induce rotation. It has three components (curl_x, curl_y, and curl_z); but in oceanography only the third component which relates to rotation around the vertical is of interest, and the index z is never written. A visualization of the relationship between Ekman pumping and wind stress curl is shown in Figure 4.2). Fig 4.3 gives a map of the annual mean of curl(τ/f) for the world ocean. Most of the ocean is characterized by Ekman transport convergence or downwelling, indicated by an extensive region of negative curl(τ/f) from the tropics to the temperate zone. Positive curl(τ/f) or upwelling is found on the poleward side of the core of the Westerlies.

The basis of Figure 4.3 is eqn (4.2), which is not defined near the equator and along boundaries. What happens there can be understood if we return to the box models of Figure 4.1. The equatorial region (box *D*) is often characterized by upwelling: In the equatorial Atlantic and eastern Pacific Oceans winds are eastward and fairly uniform; the change of sign of the Coriolis parameter across the equator produces Ekman transports of opposite signs at about 2°N and 2°S, i.e. Ekman suction and upwelling. Discussion of the situation in the equatorial Indian Ocean is left to Chapter 11 since it varies with the

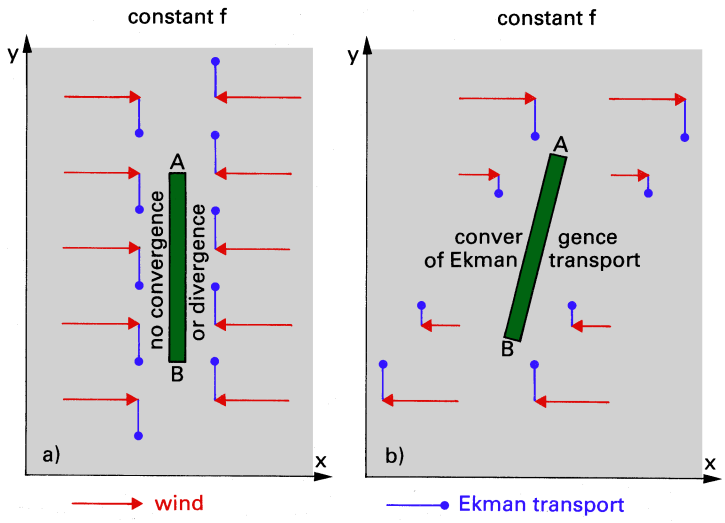

Fig. 4.2. A sketch of two wind fields and related Ekman transport, (a) with zero wind stress curl, (b) with non-zero wind stress curl. The tendency of the wind field to in-duce rotation can be visualized by the drifting balloon *AB*; it does not rotate in (a) but rotates clockwise in (b). It is seen that Ekman pumping in the ocean occurs only where rotation is present in the atmosphere. (The variation of the Coriolis parameter has been neglected to simplify matters.)

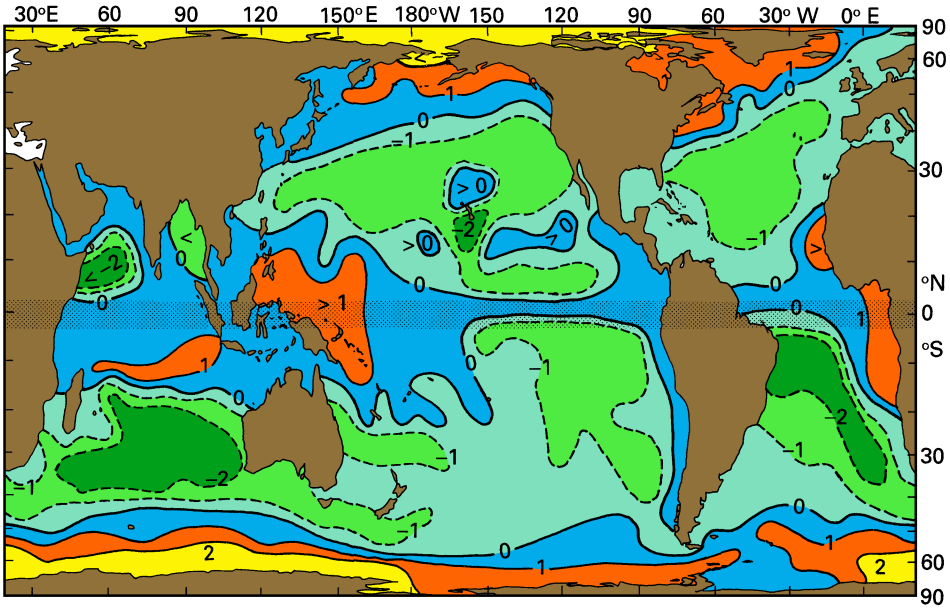

Fig. 4.3. Annual mean distribution of curl(τ/f), or Ekman pumping, calculated from the distribution of Fig. 1.4 (10^{-3} kg m^2 s^{-1}). Positive numbers indicate upwelling. In the equatorial region (2°N - 2°S, shaded) curl(τ/f) is not defined; the distribution in this region is inferred from the dynamical arguments of Fig. 4.1 and is not quantitative.

$$g\ \partial P / \partial x\ = f^2 / \beta\ \ \text{curl}\ (\tau / \rho_o f)\quad , \qquad (4.5)$$

where $$P(x,y) = \int_{z_o}^{0} h(x,y,z)\ dz \qquad (4.6)$$

has dimension m^2 and is the depth-integral of the steric height h from an assumed depth of no motion z_o to the surface: $\partial P/\partial x$ is the generalization of $H\ (\Delta\rho/\rho_o)\partial H/\partial x$ in the $1^1/_2$ layer model. Note that (4.5) is well-defined at the equator. Evaluation of the right-hand side of eqn (4.5) gives, using $\beta = df / dy$,

$$g\ \partial P / \partial x\ =\ f / (\beta\ \rho_o)\ \ \text{curl}\ (\tau)\ +\ \tau_x / \rho_o\ . \qquad (4.7)$$

All three terms in eqn (4.7) are well-defined everywhere, including the equator. The spurious "infinite" speed of Rossby waves at the equator does not affect the steady state which those waves bring about.

In the form shown in eqn (4.5), both sides of the Sverdrup relation are completely well-defined by available data - the right-hand side comes from the annual mean wind stress shown in Figure 1.4, while the left-hand side comes from the annual mean density field derived from the data shown in Figure 2.5. This provides us with a powerful means for testing the validity of our concept of ocean dynamics. How well, then, do the two sides of the Sverdrup relation match one another?

Figure 4.4 shows a global map of depth-integrated steric height calculated from atmospheric data, i.e. using the right-hand side of the Sverdrup relation (eqn (4.5)) in combination with appropriate boundary conditions to ensure that no mass flux occurs through the eastern boundary (Godfrey, 1989). The same quantity is also shown in Figures 4.5 and 4.6, this time calculated from oceanographic information, i.e. based on the left hand side of eqn (4.5) for two different depths of no motion, 1500 m and 2500 m. General agreement between the results from both data sets is observed in the subtropics. All three diagrams show a maximum value of P near the western boundary of each ocean at 30° - 40° N or S. The position of this maximum is well represented by Figure 4.4 in each basin. The number of contours from east to west in each ocean basin is fairly well represented, though the wind-based calculation produces a larger transport than the calculation based on ocean temperatures and salinities. This could be due, as has been suggested by researchers, to an inappropriately large choice of the constant C_d in the wind stress calculation of Hellerman and Rosenstein (1983).

It is also remarkable that over most of the oceans the choice of reference level for the integration of the oceanographic data fields does not influence the results very much. This indicates that flow between 1500 m and 2500 m depth is quite small, making both depths probably reasonably valid choices for a depth of no motion. Substantial differences between the strengths of the flows predicted by Figures 4.5 and 4.6 occur in the Antarctic region, indicating that at these latitudes substantial flow occurs below the 1500 m level. This aspect of the circulation will be discussed in detail in Chapter 6.

A major failing of the calculation from atmospheric data occurs west of the southern end of Africa, where it shows very strong north-south gradients of P. These gradients imply an intense geostrophic flow across the South Atlantic Ocean to South America, which then

current is seen in the southern Indian Ocean. This asymmetrical distribution of currents reflects similar asymmetries of the annual mean wind stress field of Figure 1.4.

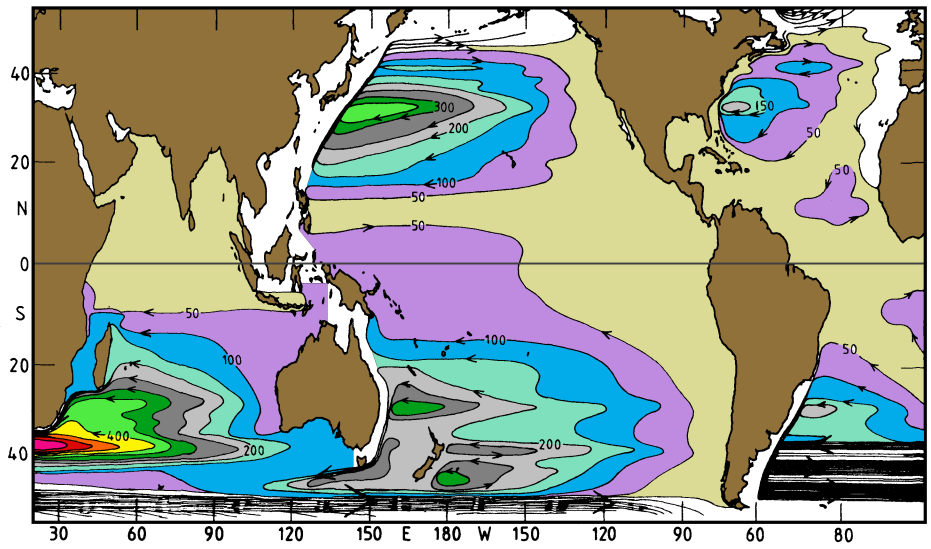

Fig. 4.4. Depth-integrated steric height P, calculated from the right-hand side of the Sverdrup relation (eqn (4.5)), using the data from Hellerman and Rosenstein (1983). Units are 10^1 m^2. For details of the integration procedure see Godfrey (1989).

An important thing to note for later reference is the magnitude of the western boundary currents generated by the Sverdrup mechanism: 50 Sv for the Kuroshio, 30 Sv for the Gulf Stream and the Brazil Current, 25 Sv for the East Australian Current, and 70 Sv for the Agulhas Current; independent estimates of the flow between Australia and Indonesia of 16 Sv were used for obtaining the latter two transports. To give some feeling what these numbers mean we note that 50 Sv correspond to about 4000 cubic kilometers per day! When it comes to the discussion of individual oceans it will become clear that none of these transport estimates is very accurate, because regional effects modify the boundary currents. Nevertheless, there can be no doubt that the currents are wind-driven, in the sense that they provide continuity of transport for the Sverdrup regime of the ocean interior.

Another feature of Figure 4.7 worth noting is the existence, in each ocean basin, of circulations bounded by contours of zero stream function value. The circulation cells bounded by zero stream function contours are known as "gyres"; those lying between the maximum westerlies and Trades in Figure 4.7 are known as the *subtropical gyres*. Within each subtropical gyre, the wind stress curl generates equatorward depth-integrated flow in the ocean interior, which returns poleward in the western boundary currents. Poleward of the subtropical gyres in the Northern Hemisphere are the *subpolar gyres*. Flow within these is poleward in the interior and equatorward at the western boundary. The convergence of the western boundary currents of the subtropical and subpolar gyres produces the *polar fronts*, regions of strong horizontal temperature and salinity gradients where warm subtropical

water meets cold subpolar water along the zero streamline contour (compare Figure 2.5). Further gyres are evident between 15°N and 10°S; they form part of the complex equatorial current system which will be discussed in later chapters and are not usually recognized as gyres by name.

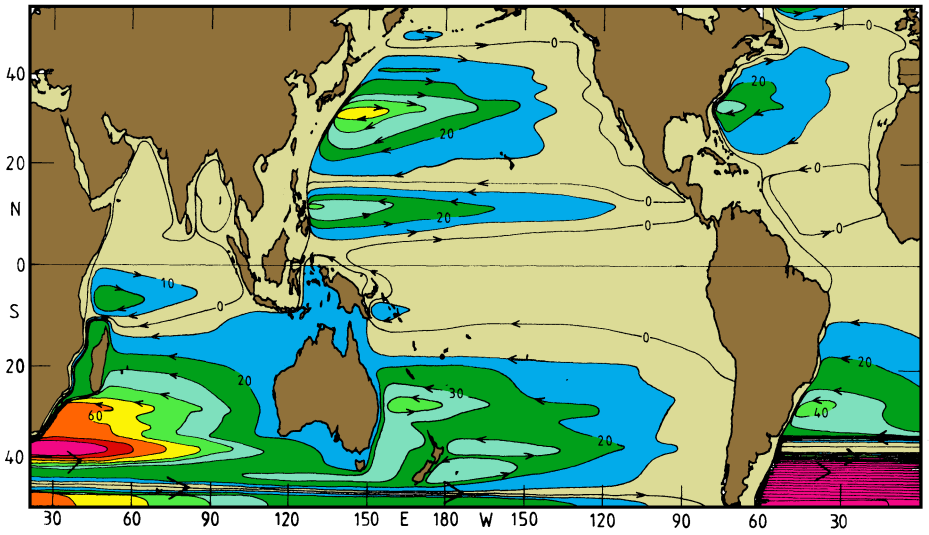

Fig. 4.7. Stream function for the world ocean, calculated from the wind stress data of Hellerman and Rosenstein (1983). Contour interval is 10 Sv.

It can be shown that if the winds were purely zonal and did not vary with longitude, the zero stream function contours would coincide with zero contours of wind stress curl. In other words, subject to the same assumptions, the boundaries of the gyres would coincide with the maximum westerly wind stresses, and with the maximum Trades. Purely zonal winds with no longitudinal variation are of course a somewhat poor description of the real mean winds; but the assumption is useful as a first approximation. The lines of zero stream function in Figure 4.7 do indeed either lie close to the maximum westerlies, or the maximum Trades, as can be seen by comparison with Figure 1.2.

Since the depth-integrated flow cannot cross streamlines, there is no *net* transport of mass between adjacent gyres (provided, that is, that the conditions of the Sverdrup circulation are met). This does not mean, however, that no water crosses from one gyre into another. In fact, transport in the surface layer across zero streamlines is maximum because the zonal wind stresses along these boundaries - and as a consequence the Ekman transport - are at a maximum. The surface layer transport is balanced by geostrophic transport below, so the *net* transport is zero. At the equatorward boundary of the subtropical gyres the Ekman transport is directed poleward and moves warm water away from the tropics, while the compensating deep geostrophic flow brings cold water into the tropics. Thus, although there is no net mass transport across the zero stream function contour, there is substantial

restricted our survey to a square of some 200 km base length we could find it very difficult to recognize the mean flow. The water in the ocean is constantly mixed, a major mixing mechanism being eddy mixing. Figure 4.8 shows mean eddy energy in the ocean. The western boundary currents (Gulf Stream, Brazil Current, Kuroshio, East Australian Current, Agulhas Current) and the Circumpolar Current stand out as regions of particularly high eddy energy. Eddies in these regions are so energetic that the associated currents can reverse the direction of flow. In the western boundary currents they turn the water movement from poleward to equatorward; poleward mean flow is only observed if the study area is larger than the typical eddy size, which is of the order of 200 km diameter. Away from the boundary currents eddy energy goes down rapidly; but annual mean velocities decrease as well, and eddies can still reverse the observed direction of mean flow if the study area is too small. Figure 4.9 demonstrates this for the area of the Azores Current in the eastern north Atlantic Ocean. In the example the cruise covered an area of roughly 550 · 550 km with 86 stations. At least three eddies are seen, but the Azores Current is still visible meandering through the region between the eddies. A smaller study area would not show much resemblance between the annual mean and the actual situation.

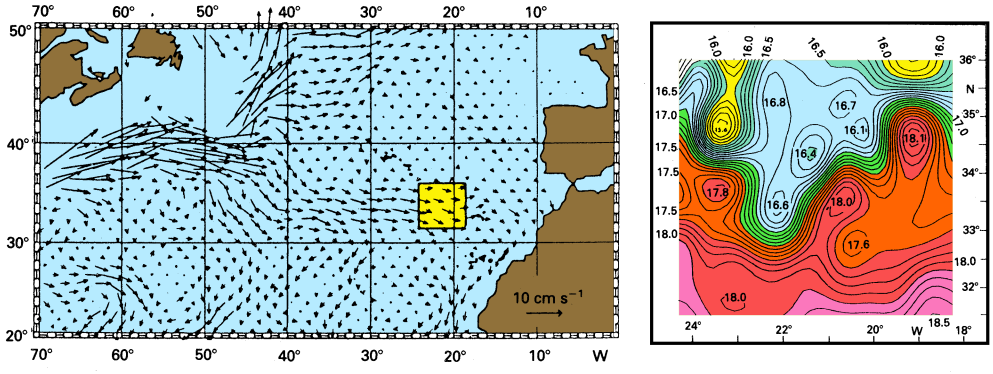

Fig. 4.9. Eddies in the Azores Current. (a) Mean surface flow based on historical data. (b) The box of panel (a) enlarged, showing the Azores Current and eddies as indicated by the temperature of the surface mixed layer, during April 1982. (Horizontal temperature gradients indicate a sloping interface and associated eddies in the manner of Fig. 3.3.) From Käse *et al*. (1985).